PIER C

Design of Permanent Magnet Synchronous Wind Power Control System

Huajun Ran, Wenjin Wei*, and Yue Gao

College of Electricity & New Energy, China Three Gorges University, Yichang, Hubei 44300, China

ABSTRACT: To tackle the slow response and insufficient interference resistance exhibited by permanent magnet synchronous motors (PMSMs) under traditional field-oriented control (FOC). This paper proposes an integral sliding mode controller (SMC) to improve the speed loop, and adaptive law is also developed using a nonlinear smooth function to eliminate the chattering phenomenon of the sliding mode control. Meanwhile, an extended state observer is designed to estimate and compensate for the disturbances caused by wind speed uncertainty and system's internal disturbances. Then, model predictive control (MPC) is employed for the current loop to eliminate the overshoot and achieve fast tracking. Finally, a step-by-step model reference adaptive scheme (MRAS) is proposed to identify the parameters and eliminate the internal disturbances in addressing parameter perturbation in the motor during operation. The simulation results demonstrate that the enhanced system exhibits almost no overshoot, superior steady-state performance, quick dynamic response, and resistance to both internal and external disturbances, ultimately validating the efficacy of the approach.

1. INTRODUCTION

The three-phase permanent magnet synchronous motor is widely utilized for its straightforward construction, convenient operation, and high power efficiency. Thus, direct-drive wind turbines with PMSM have become the mainstay of the wind power market [1, 2].

Generally, a high-performance PMSM drive system requires a fast response loop to ensure that the motor response strictly tracks the change of the reference value, thereby ensuring stability, high precision, and high dynamic performance [3]. Optimal motor control performance is achieved by improving the control strategy of the PMSM control system. Currently, the traditional double-layer nested proportional-integral (PI) loop structure with FOC is widely used in which the double loop separately controls the speed and current [4, 5]. The methods to improve PI control proposed by scholars include fuzzy control [6], sliding mode control [7], robust control [8], and model predictive control [9]. However, in a wind power system, the speed loop directly affects the effect of maximum power point tracking (MPPT) [10], and the motor rotational speed is also directly affected by the wind conditions. Meanwhile, considering that wind speed has the characteristics of randomness, time variability, and mutation [11], a control strategy insensitive to external disturbances is required. Among them, sliding mode control is suitable for application in this background because of its advantages of fast response and insensitivity to parameter changes and disturbances [12].

Secondly, to eliminate the uncertainty of the wind power system and improve speed tracking ability, a nonlinear extended state observer is designed to estimate and compensate the uncertainty [13]. However, the chattering phenomenon of the sliding mode controller limits its development [14]. A nonlinear smoothing function is introduced to design the sliding mode reaching law, fundamentally eliminating the chattering phenomenon.

The current loop is the core component of the control system, which directly affects the dynamic performance of the control system [15]. The traditional current-PI loop is stable, reliable, and simple in structure. However, the parameter robustness is poor, which cannot meet the performance requirements of fast and accurate PMSM responses in the considerable current range [16]. Model predictive control (MPC) measurement has recently attracted much attention in many fields [17]. The basic idea of MPC is to predict future action by discretizing the mathematical model [18]. The model prediction control methods used in the current loop are divided into model predictive current control (MPCC) and deadbeat predictive current control (DPCC) [19]. The former selects the minimum value of the cost function as the next time output by calculating the voltage space vector [20]. Meanwhile, there are studies to reduce the amount of calculation and improve the running speed by using double-vector or three-vector measurements [21, 22]. With the widespread adoption of multi-level converters, the quantity of space vectors expands, and the sharp increase in calculation will seriously affect the application of MPCC [23]. However, the DPCC generates the control amount through the SVPWM module, which is simple and reliable.

Most importantly, DPCC is fast in tracking, simple in modeling, great in robustness, and with no static error, which can obtain a better dynamic response [24]. This paper applies DPCC to improve the current loop. However, DPCC relies heavily on the accurate mathematical model of the system. Therefore, it is necessary to monitor the crucial parameters online. The traditional online parameter identification methods mainly include recursive least squares method (RLS), model reference

---

* Corresponding authors: Wenjin Wei (1246778415@qq.com).

adaptive scheme (MRAS), and extended Kalman filter [25]. RLC and Kalman filter methods are data-dependent, and significant errors exist when the velocity undergoes frequent changes. In contrast, the MRAS identification effect performs well but faces an issue with deficiency ranking, leading to the identification results being prone to becoming trapped in local solutions. This paper adapts an improved MRAS identification method to solve this problem. Finally, the simulation model is established in the Matlab/Simulink environment and compared with the double-PI and double-MPC control strategies.

This paper makes the following contributions:

1) The integral sliding mode controller replaces the speed PI loop, and a nonlinear smoothing function constructs the sliding mode reaching law to eliminate the chattering phenomenon of the sliding mode fundamentally.

2) The extended state observer observation is designed to actively estimate and compensate for the uncertain factors caused by wind conditions and improve the tracking ability of the speed loop.

3) The simple DPCC is selected as the current loop, significantly saving the calculation and dramatically weakening the steady-state torque ripple and current harmonics compared with the double-MPC model.

4) An improved MRAS method is used to solve the problem of deficiency rank.

The layout of this paper is as follows. The second section introduces the two-phase rotating coordinate system PMSM wind power system and its mathematical model. The third section first introduces the integral sliding mode observer and the extended state observer of the improved speed loop. The following part introduces the DPCC and MRAS models with step-by-step identification. The fourth section presents the model parameters, builds the simulation, and verifies the method proposed in this paper.

2. PERMANENT MAGNET SYNCHRONOUS WIND POWER SYSTEM

2.1. Wind Turbine Model

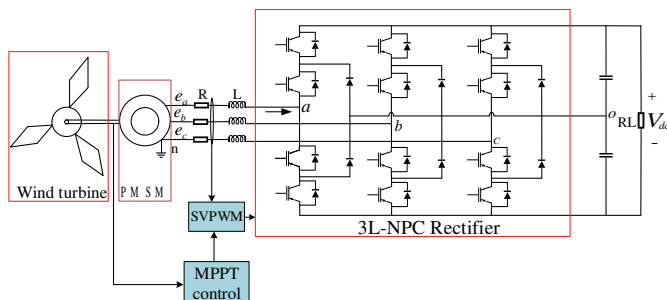Firstly, the topology diagram of the PMSM wind power system is introduced as follows (Figure 1):

FIGURE 1. PMSM wind power systems.

In the wind turbine model, the mechanical power (P_m), mechanical torque (T_m), and speed of a wind turbine (ω_r) are closely related to the wind speed (V_w). Nevertheless, in direct-drive synchronous wind turbines, the wind turbine is directly connected to the motor. Thus, there is also the relationship: $\omega_r = \omega_m$. According to the Bates theory, the above parameters have the following relationship:

$$\begin{cases} P_m = \rho \pi R^2 C_p V_m^3 / 2 \\ T_m = P_m / \omega_r = \dfrac{1}{2\lambda^3} \rho \pi R^5 C_p \omega_r^2 \\ \lambda = R\omega_r / V_m \end{cases} \tag{1}$$

where ρ is the air density, R the radius of wind turbine blades, C_p the maximum wind energy utilization factor with a maximum value of 0.48, and λ the optimal tip speed ratio.

Therefore, achieving MPPT necessitates calculating the ideal velocity and torque to efficiently utilize wind energy while ensuring that the tip speed ratio is optimal.

2.2. PMSM Model

The mathematical model of the PMSM is described by the two-phase synchronous rotating dq coordinate system:

$$\begin{cases} u_d = R_s i_d + \dfrac{d\psi_d}{dt} - \psi_q \omega_m \\ u_q = R_s i_q + \dfrac{d\psi_q}{dt} - \psi_d \omega_m \end{cases} \tag{2}$$

Here u_d and u_q are the stator voltage in the dq coordinate system; i_d and i_q are the stator current components; ψ_d and ψ_q are the dq-axis flux components; R_s is the stator side resistance; ω_m is the rotor angular velocity.

The magnetic flux equation can be expanded as follows:

$$\begin{cases} \psi_d = L_d i_d + \psi_f \\ \psi_q = L_q i_q \end{cases} \tag{3}$$

Among them, $\omega_m = n_p \omega_g$, and the PMSM equation is rewritten as:

$$\begin{cases} \dfrac{di_d}{dt} = -\dfrac{R_s}{L_d} + n_p \omega_g i_q + \dfrac{u_d}{L_d} \\ \dfrac{di_q}{dt} = -\dfrac{R_s}{L_q} + n_p \omega_g i_d + \dfrac{u_q}{L_q} - \dfrac{n_p \psi_f}{L_q} \omega_g \end{cases} \tag{4}$$

where n_p is the number of pole pairs of the motor, and ω_g indicates the motor rotor speed. ψ_f is the flux linkage of the permanent magnet.

The direct-drive wind turbine model typically employs a surface permanent magnet synchronous motor, and there is a relationship of $L_d = L_q = L$. Then, to better control the active power input of PMSM, the zero d-axis current control strategy is assumed: The d-axis component reference value of the stator

current is set as that during the operation, and the expression of the electromagnetic torque is obtained as follows:

$$T_e = 1.5 n_p \psi_f i_q \tag{5}$$

The mechanical motion equation of the motor is:

$$J \frac{d\omega_m}{dt} = T_e - T_m - B\omega_m \tag{6}$$

According to Eq. (5) and Eq. (6), the dynamic state equation of the transmission shaft system of the wind power system can be obtained as follows:

$$\dot{\omega}_g = \frac{1}{J}(T_m - 1.5 n_p \psi_f i_q - B_m \omega_g) \tag{7}$$

where T_e is the electromagnetic torque, J the rotational inertia, and B_m the damping coefficient.

3. IMPROVE THE FOC STRATEGY

3.1. Speed Controller

Considering that wind energy has time-varying uncertainty, it is beneficial to utilize an expanded state observer for estimating and compensating uncertainties and disturbances when designing an integral sliding mode controller. Firstly, an extended state observer is designed to compensate the disturbances.

The dynamic state Eq. (7) of the transmission shaft system of the wind power generation system is expanded:

$$\dot{\omega}_g = \frac{T_m}{J} - \frac{1.5 n_p \psi_f}{J} i_q - \frac{B_m}{J} \omega_g \tag{8}$$

Let $x_1 = \omega_g$, $x_2 = \frac{T_m}{J} - \frac{B_m}{J} \omega_g$, $b = -\frac{1.5 n_p \psi_f}{J}$ and $u = i_q$, where x_1 x_2 are the extended state variables; u is the system control input; y is the system output, then the dynamic equation of the drive shaft can be extended as:

$$\begin{cases} \dot{x}_1 = x_2 + bu \\ \dot{x}_2 = w \\ y = x_1 \end{cases} \tag{9}$$

According to Eq. (9), the second-order extended state observer is constructed as follows:

$$\begin{cases} e_1 = z_1 - y \\ \dot{z}_1 = z_2 - \beta_1(e_1 + g(e_1, \delta_1)) + bu \\ \dot{z}_2 = -\beta_2(e_1 + g(e_1, \delta_2)) \end{cases} \tag{10}$$

According to the literature [29], a better nonlinear function is:

$$g(x, \delta) = \frac{x}{\delta^2} \exp\left(-\frac{x^2}{2\delta^2}\right) \tag{11}$$

In the observer, β_1 and β_2 are the observation error gain parameters, and δ_1 and δ_2 are the observation error immune factors. An observer with accurate state estimation can be designed with reasonable design parameters. The extended state

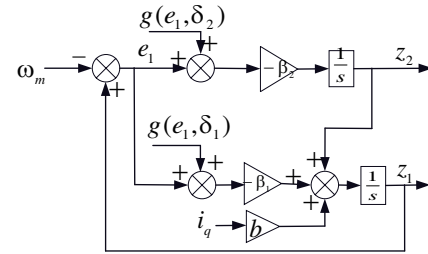observer block diagram constructed by the nonlinear function is as follows (Figure 2):

FIGURE 2. Extended state observer block diagram.

When designing the sliding mode controller, set the tracking error to $e(t) = \omega_{ref} - \omega_g$, then according to the extended state Eq. (9) can obtain:

$$\dot{e}(t) = -\dot{\omega}_g = -\dot{x}_1 = -x_2 - bu \tag{12}$$

In this paper, an integral sliding mode controller is introduced. By placing the system's initial state on the sliding mode surface, the additional time required to reach the sliding mode surface can be eliminated, and the robustness of the control system is also improved. The integral sliding mode function is designed as follows:

$$s = c_0 \int_{-\infty}^{t} e(t)dt + e(t) \tag{13}$$

The sliding mode reaching law is designed as follows:

$$\dot{s} = -c_1 s - c_2 g(s, \delta_3) \tag{14}$$

The sliding mode control law is:

$$u = \frac{c_0(\omega_{ref} - x_1) - x_2 + c_1 s + c_2 g(s, \delta_3)}{b} \tag{15}$$

Based on Eq. (15), the sliding mode control law can be redefined with the extended state observer:

$$u = \frac{c_0(\omega_{ref} - z_1) - z_2 + c_1 s + c_2 g(s, \delta_3)}{b} \tag{16}$$

In summary, according to the sliding mode controller and nonlinear extended state observer (NLESO) designed above, the improved speed loop structure diagram is as follows (Figure 3):
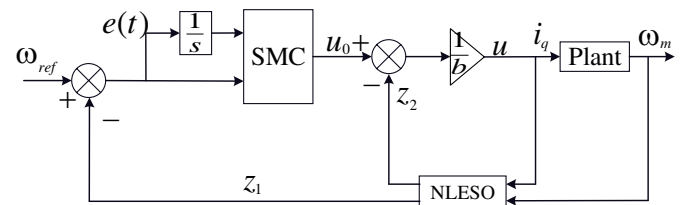

FIGURE 3. Integral sliding mode controller combined with observer.

Stability analysis: According to the reaching law, which can be obtained when $s = 0$, $\dot{V} = s \cdot \dot{s} = 0$. When $s \neq 0$ as long as the inequality is satisfied:

$$c_1 |s| + c_2 |g(s, \delta_3)| \geq c_0 d_1 + d_2 \tag{17}$$

Based on the above equation $\dot{V} = s \cdot \dot{s} \leq 0$, the Lyapunov function $V(s)$ is always positive definite, and $\dot{V}$ is negative definite, which satisfies the stability theorem, making the sliding mode system widely stable.

The improved method of speed loop can enhance the speed tracking efficiency and eliminate the unknown disturbances inside and outside the system during operation. Additionally, since the sliding mode controller is not sensitive to parameter perturbations, it can ignore the problem of parameter perturbations. In summary, this method improves the tracking effect of the speed loop and has good anti-disturbance performance and strong robustness, which can also provide a solid basis for the design of the current loop.

3.2. Current Controller

In the FOC control system, the current loop is the crucial factor affecting the dynamic and static performance. In the cause of improving the poor tracking effect of the PI control, DPCC is used to track the current, which uses the given current value to directly predict the voltage required by the system without adjusting the weight parameters. Compared with the double-MPC model predictive control scheme adopted in [30], DPCC has better dynamic performance, minor current ripple, lower torque ripple, and higher current frequency response.

According to the mathematical model of Eq. (4), the stator current of the motor is selected as the state variable, and the following formula can be obtained:

$$\frac{di}{dt} = Ai + Bu + D \qquad (18)$$

where $A = \begin{bmatrix} -R/L & \omega_m(k_i) \\ -k_i & -R/L \end{bmatrix}$, $B = \begin{bmatrix} 1/L & 0 \\ 0 & 1/L \end{bmatrix}$,

$D(k_i) = \begin{bmatrix} 0 \\ -\psi_f \omega_m(k_i)/L \end{bmatrix}$, $i = \begin{bmatrix} i_d \\ i_q \end{bmatrix}$ and $u = \begin{bmatrix} u_d \\ u_q \end{bmatrix}$.

Because the control period T_i of the current inner loop is short enough, the input voltage u and reverse potential D are considered constant in the control period $[k_i T_i, k_{i+1} T_{i+1}]$. Based on the Euler discretization solution, the model of the predicted current is:

$$i(k_{i+1}) = F(k_i) \cdot i(k_i) + G \cdot u(k_i) + H(k_i) \qquad (19)$$

where $i(k_i) = \begin{bmatrix} i_d(k_i) \\ i_q(k_i) \end{bmatrix}$, $u(k_i) = \begin{bmatrix} u_d(k_i) \\ u_q(k_i) \end{bmatrix}$,

$F(k_i) = \begin{bmatrix} 1 - T_i R/L & T_i \omega_m(k_i) \\ -T_i \omega_m(k_i) & 1 - T_i R/L \end{bmatrix}$, $G = $

$T_i \cdot B = \begin{bmatrix} T_i/L & 0 \\ 0 & T_i/L \end{bmatrix}$, $H(k_i) = T_i \cdot D(k_i) = $

$\begin{bmatrix} 0 \\ -T_i \psi_f \omega_m(k_i)/L \end{bmatrix}$.

The basic idea of DPCC is to first sample the current value at $k_i T_i$, then predict the voltage value applied at the current time

according to the current prediction model. Thus, the current sample at $k_{i+1} T_{i+1}$ is tracked to a given deadbeat current value.

$$\begin{cases} i_d(k_{i+1}) = i_d^*(k_i) \\ i_q(k_{i+1}) = i_q^*(k_i) \end{cases} \qquad (20)$$

where $i_d^*(k_i)$ and $i_q^*(k_i)$ are the reference values of the dq axis at the moment k_i.

In this process, to make the actual current of PMSM follow the reference value in the next current cycle, the speed loop output at $k_i T_i$ is set as the current reference value $i(k_{i+1})$. Therefore, the rapid tracking of the speed loop also creates conditions for the stability of the current loop. The current operating state value $i(k_i)$ obtained by current sampling is substituted into the Euler discrete prediction model to calculate the voltage vector $u(k_i)$ required to make the current accurately follow the instructions.

$$u(k_i) = G^{-1} \left[i^*(k_{i+1}) - F(k_i)i(k_i) - H(k_i) \right] \qquad (21)$$

Among them, $i^*(k_{i+1})$ is the given current value at $k_{i+1} T_{i+1}$. Because the sampling time is very short, it can be considered that the given current value at $k_{i+1} T_{i+1}$ is equal to that at $k_i T_i$. Then, the approximate relationship $i^*(k_{i+1}) \approx i^*(k_i)$ can be obtained. Finally, the above equation is simplified as follows:

$$u(k_i) = G^{-1} \left[i^*(k_i) - F(k_i)i(k_i) - H(k_i) \right] \qquad (22)$$

Finally, according to the principle of FOC control, the obtained voltage vector generates a switching signal through the SVPWM module to control the rectifier.

To summarise, replacing the current PI loop with DPCC can improve the static and dynamic response of the system. Nonetheless, during the actual operation, the motor's operating parameters tend to fluctuate, which can ultimately influence the performance of the current loop. Therefore, the MRAS is used to identify the parameters to eliminate the poor tracking effect caused by the parameter mismatch. In addition, to solve the deficiency-rank problem in the traditional MRAS, the step-by-step parameter identification method is used to identify the flux linkage, resistance, and inductance, respectively. The specific ways are as follows:

1) Set the initial value of the identification parameters:

$\widehat{\psi}_f(0), \widehat{L}(0)$ and $\widehat{R}(0)$.

2) Based on the motor's voltage state equation, the flux linkage solely depends on the q-axis. Hence, the adjustable model of the flux linkage is designed using the q-axis voltage equation, while the Popov theorem is utilized to design the adaptive law of the flux linkage, thus accomplishing the identification of the flux linkage.

3) The identified flux linkage serves as a known quantity and is introduced into the voltage equation of state and the inductance and resistance are identified similarly. Finally, the identified values for resistance and inductance are entered into the flux linkage identification model.

The above steps are repeated until the identification is stable.

Firstly, according to Eq. (4), the q-axis current state equation is set as the reference model:

$$\frac{di_q}{dt} = \frac{u_q}{L} - \frac{R_s i_q}{L} - \omega_e i_d - \frac{\omega_e \psi_f}{L} \qquad (23)$$

The corresponding adjustable model is designed as follows:

$$\frac{d\widehat{i}_q}{dt} = \frac{u_q}{L} - \frac{\widehat{R}_s \widehat{i}_q}{L} - \omega_e i_d - \frac{\omega_e \widehat{\psi}_f}{L} \qquad (24)$$

The first-order current error system can be obtained by subtracting the above two current equations. The adaptive law is designed based on the Popov hyperstability, and the adaptive law of the rotor flux linkage is set to the proportional form:

$$\widehat{\psi}_f = \int_0^t g_1(\tau)d\tau + g_2(t) + \widehat{\psi}_f(0) \qquad (25)$$

$$\int_0^{t_1} (i_q - \widehat{i}_q)\frac{\omega_e}{L}(\psi_f - \widehat{\psi}_f)dt \geq -\gamma^2 \qquad (26)$$

When the system is globally stable, $g_1(\tau)$ and $g_2(t)$ can be set as:

$$\begin{cases} g_1(\tau) = -k_i(i_q - \widehat{i}_q)\dfrac{\omega_e}{L} \\[2mm] g_2(\tau) = -k_p(i_q - \widehat{i}_q)\dfrac{\omega_e}{L} \end{cases} \qquad (27)$$

The flux adaptive law can be obtained as:

$$\widehat{\psi}_f = -\left(\frac{k_i}{s} + k_p\right)(i_q - \widehat{i}_q)\frac{\omega_e}{L} + \widehat{\psi}_f(0) \qquad (28)$$

Based on the above formula, the estimated value $\widehat{\psi}_f$ of the flux linkage can be obtained.

After identifying the flux linkage, it is utilized as a known parameter to calculate the inductance and resistance. Based on the PMSM voltage equation, the reference model is:

$$\frac{d}{dt}\begin{bmatrix} i_d \\ i_q \end{bmatrix} = \begin{bmatrix} -\frac{R_s}{L} & \omega_e \\ -\omega_e & -\frac{R_s}{L} \end{bmatrix}\begin{bmatrix} i_d \\ i_q \end{bmatrix}$$
$$+ \begin{bmatrix} \frac{1}{L} & 0 \\ 0 & \frac{1}{L} \end{bmatrix}\begin{bmatrix} u_d \\ u_q \end{bmatrix} + \begin{bmatrix} 0 \\ -\frac{\omega_e \psi_f}{L} \end{bmatrix} \qquad (29)$$

The adjustable model is written as follows:

$$\frac{d}{dt}\begin{bmatrix} \widehat{i}_d \\ \widehat{i}_q \end{bmatrix} = \begin{bmatrix} -\frac{\widehat{R}_s}{L} & \omega_e \\ -\omega_e & -\frac{\widehat{R}_s}{L} \end{bmatrix}\begin{bmatrix} i_d \\ i_q \end{bmatrix}$$
$$+ \begin{bmatrix} \frac{1}{\widehat{L}} & 0 \\ 0 & \frac{1}{\widehat{L}} \end{bmatrix}\begin{bmatrix} u_d \\ u_q \end{bmatrix} + \begin{bmatrix} 0 \\ -\frac{\omega_e \psi_f}{\widehat{L}} \end{bmatrix} \qquad (30)$$

The second-order error system can be obtained by subtracting the voltage equation.

Similar to the flux linkage identification process, the adaptive law of inductance and resistance is set to the proportional form according to the Popov hyperstability, and the adaptive law of resistance and inductance is finally obtained:

$$\begin{cases} \widehat{R}_s = \dfrac{-\left(\frac{k_i'}{s}+k_p'\right)[(i_d-\widehat{i}_d)\widehat{i}_d+(i_q-\widehat{i}_q)\widehat{i}_q]+\frac{\widehat{R}_s}{\widehat{L}}}{\left(\frac{k_i''}{s}+k_p^i\right)[(i_d-\widehat{i}_d)u_d+(i_q-\widehat{i}_q)u_q-(i_q-\widehat{i}_q)\omega_e\psi_f+\frac{1}{\widehat{L}}(0)]} \\[4mm] \widehat{L} = \dfrac{1}{\left(\frac{k_i''}{s}+k_p^i\right)[(i_d-\widehat{i}_d)u_d+(i_q-\widehat{i}_q)u_q-(i_q-\widehat{i}_q)\omega_e\psi_f+\frac{1}{\widehat{L}}(0)]} \end{cases}$$
$$(31)$$

In summary, the estimated values of flux linkage, inductance, and resistance can be obtained step by step. The identification process is shown in Fig. 4.

Through the above steps, the control system block diagram can be rewritten as in Fig. 5.

4. SIMULATION AND RESULTS

In order to assess the efficacy of the proposed control method, it is compared with the traditional double-PI and advanced double-MPC control strategies. Simulations are conducted utilizing the Simulink Environment of Matlab, and the different control strategies are compared under the step wind, gradual wind, and random wind conditions. Finally, the analysis mainly focuses on the tracking effect of the current loop and speed loop.

The system simulation parameters are as follows (Table 1):

TABLE 1. System Parameters.

Parameters	Values	Unit
Pole Number	4	
Flux Linkage	0.175	Wb
Stator Resistance	0.2	Ω
Stator Inductance	0.002	H
Rotational Inertia	0.05	kg·m²
Capacitor	0.0335	F
Frequency	10000	Hz

Firstly, it is verified under step wind, and the wind speed jumps from 8 m/s to 12 m/s at 0.5 s. The generator speed tracking comparison diagrams of double-PI, double-MPC, and the SMC-MPC proposed in this paper are as in Fig. 6.

According to the above figure, when the motor starts, the rotation speed under double-PI and double-MPC control has an overshoot, and the static error is more significant than SMC-MPC. Then, when the wind speed step is at 0.5 s the double-PI control tracking speed is faster, but the overshoot is significant, and the stabilization time is extended. Although the double-MPC control method has no overshoot, the tracking speed is slower than SMC-MPC.

The dq-axis current fluctuation is as in Fig. 7.

The current fluctuation under double-PI control is significant in the steady state, and the tracking effect is general. The double-MPC tracking ability is better than double-PI control but much worse than the SMC-MPC. When the step occurs,
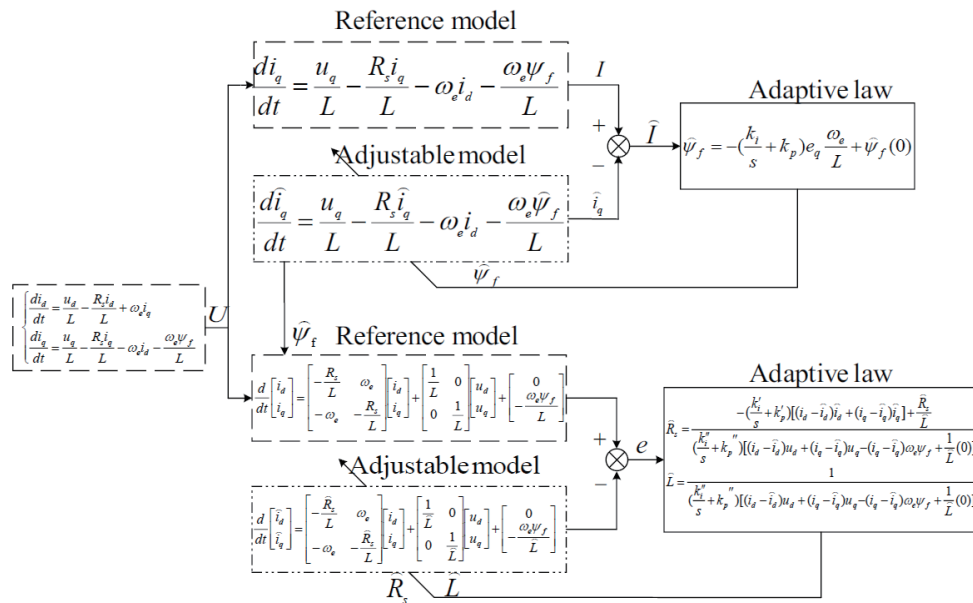
Reference model

$$\left|\frac{di_q}{dt} = \frac{u_q}{L} - \frac{R_s i_q}{L} - \omega_e i_d - \frac{\omega_e \psi_f}{L}\right|$$

Adjustable model

$$\left|\frac{d\hat{i}_q}{dt} = \frac{u_q}{L} - \frac{R_s \hat{i}_q}{L} - \omega_e i_d - \frac{\omega_e \hat{\psi}_f}{L}\right|$$

$$\left|\begin{array}{l}\frac{di_d}{dt} = \frac{u_d}{L} - \frac{R_s i_d}{L} + \omega_e i_q \\ \frac{di_q}{dt} = \frac{u_q}{L} - \frac{R_s i_q}{L} - \omega_e i_d - \frac{\omega_e \psi_f}{L}\end{array}\right| \quad U$$

Adaptive law

$$\hat{\psi}_f = -\left(\frac{k_i}{s} + k_p\right)e_q \frac{\omega_e}{L} + \hat{\psi}_f(0)$$

Reference model

$$\frac{d}{dt}\begin{bmatrix} i_d \\ i_q \end{bmatrix} = \begin{bmatrix} -\frac{R_s}{L} & \omega_e \\ -\omega_e & -\frac{R_s}{L} \end{bmatrix}\begin{bmatrix} i_d \\ i_q \end{bmatrix} + \begin{bmatrix} \frac{1}{L} & 0 \\ 0 & \frac{1}{L} \end{bmatrix}\begin{bmatrix} u_d \\ u_q \end{bmatrix} + \begin{bmatrix} 0 \\ -\frac{\omega_e \psi_f}{L} \end{bmatrix}$$

Adjustable model

$$\frac{d}{dt}\begin{bmatrix} \hat{i}_d \\ \hat{i}_q \end{bmatrix} = \begin{bmatrix} -\frac{\bar{R}_s}{L} & \omega_e \\ -\omega_e & -\frac{\bar{R}_s}{L} \end{bmatrix}\begin{bmatrix} i_d \\ i_q \end{bmatrix} + \begin{bmatrix} \frac{1}{L} & 0 \\ 0 & \frac{1}{L} \end{bmatrix}\begin{bmatrix} u_d \\ u_q \end{bmatrix} + \begin{bmatrix} 0 \\ -\frac{\omega_e \psi_f}{L} \end{bmatrix}$$

Adaptive law

$$\bar{R}_s = \frac{-\left(\frac{k_i'}{s} + k_p'\right)\left[(i_d - \hat{i}_d)\hat{i}_d + (i_q - \hat{i}_q)\hat{i}_q\right] + \frac{\bar{R}_s}{L}}{\left(\frac{k_i''}{s} + k_p''\right)\left[(i_d - \hat{i}_d)u_d + (i_q - \hat{i}_q)u_q - (i_q - \hat{i}_q)\omega_e \psi_f + \frac{1}{L}(0)\right]}$$

$$\bar{L} = \frac{1}{\left(\frac{k_i''}{s} + k_p''\right)\left[(i_d - \hat{i}_d)u_d + (i_q - \hat{i}_q)u_q - (i_q - \hat{i}_q)\omega_e \psi_f + \frac{1}{L}(0)\right]}$$

$\bar{R}_s \quad \bar{L}$

FIGURE 4. MRAS parameter identification flow chart.
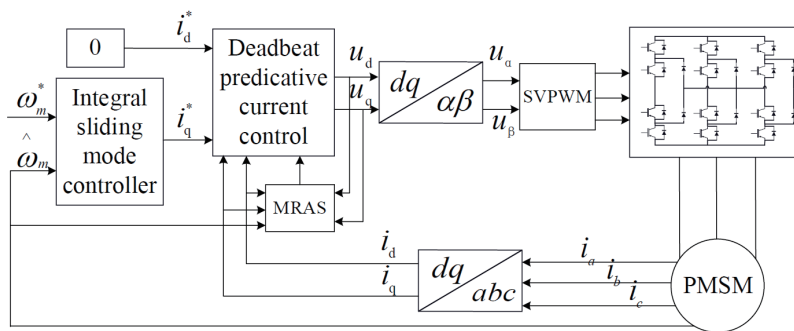
FIGURE 5. Improved PMSM control block diagram.

Comparison of speed in different control modes
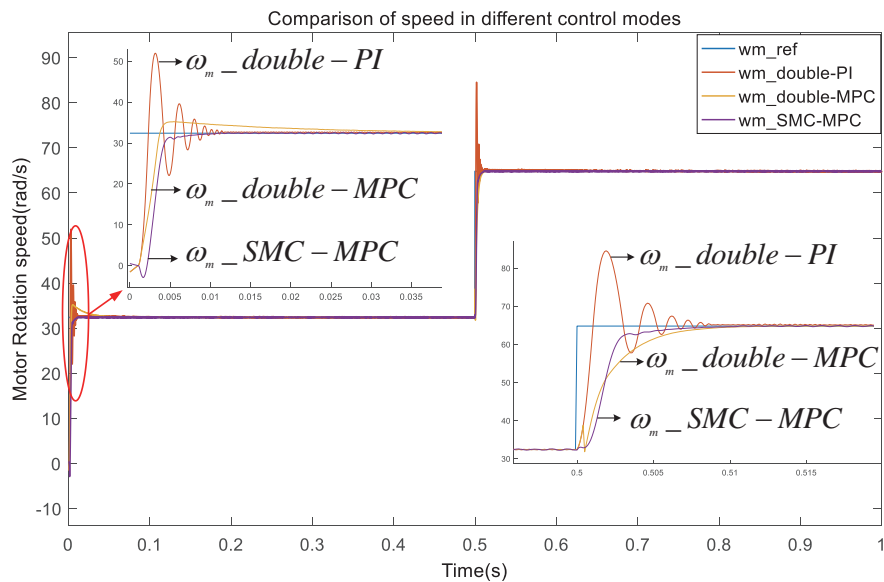

FIGURE 6. Rotation speed relationship under three control strategies under step wind.
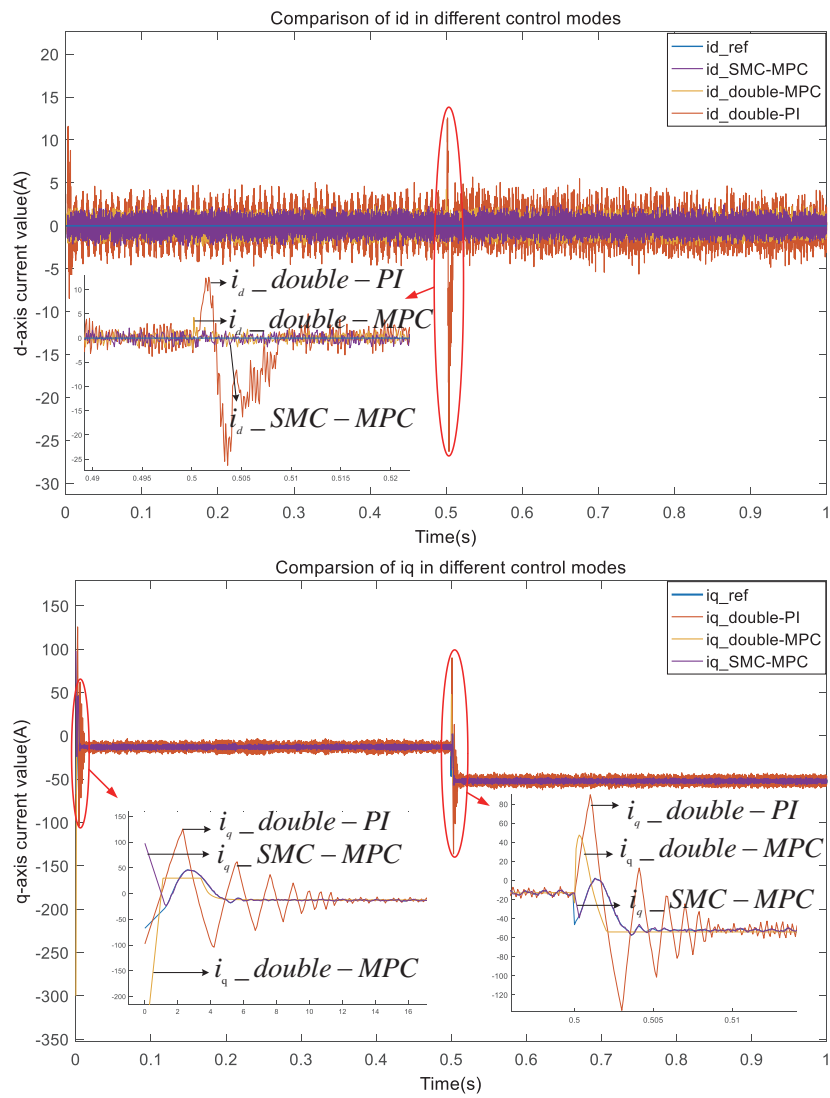
FIGURE 7. dq-current relationship under three control strategies under step wind.
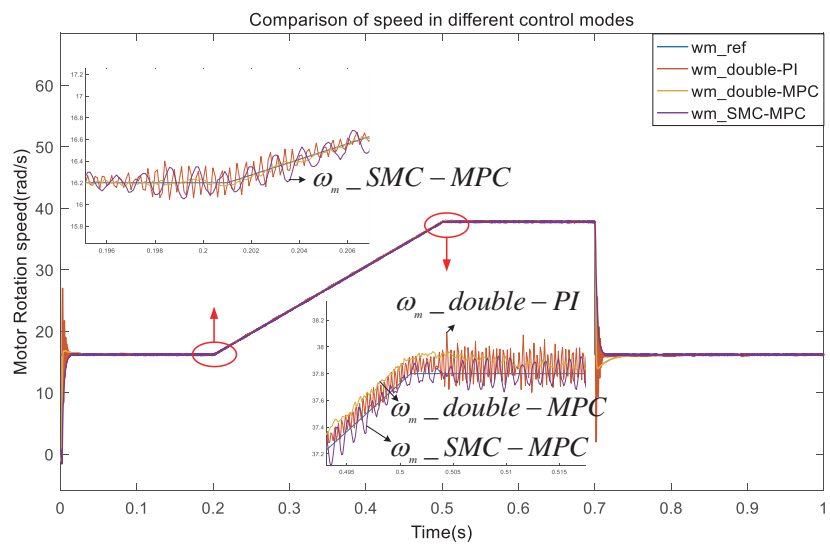

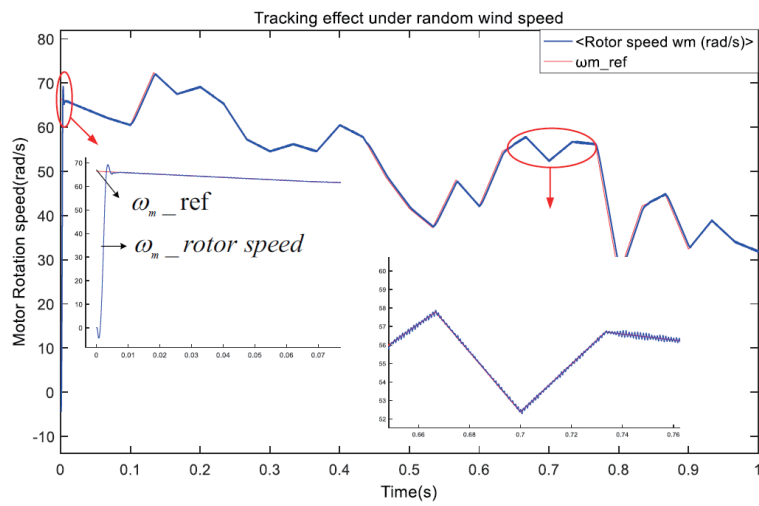**FIGURE 8**. Rotation peed relationship under three control strategies under gradient wind.

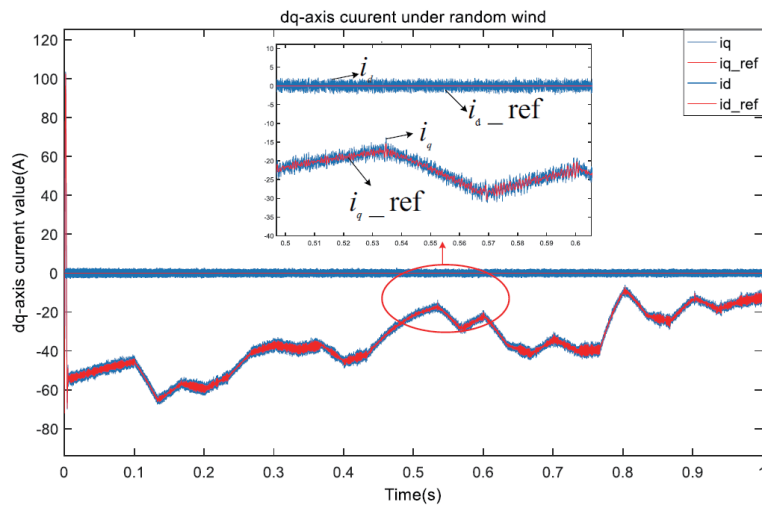**FIGURE 9**. Rotation speed relationship under three control strategies under the random wind.

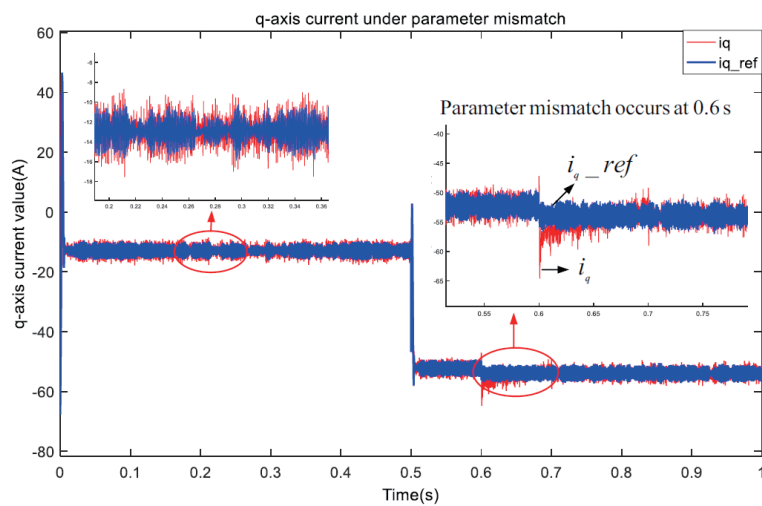**FIGURE 10**. dq-current under the random wind.

FIGURE 11. q-axis current under the parameter identification process.

the double-PI control fluctuates wildly, and the double-MPC also has an overshoot when the step occurs. The SMC-MPC can closely follow the current change without overshooting and track quickly.

The above simulation results show that SMC-MPC has a fast response speed and great dynamic performance under step wind speed. Moreover, the dynamic performance of the speed loop will also affect the current loop, so the double loop's improvement can improve the system's performance.

Secondly, it is verified under the gradient wind speed: the wind speed starts to increase from the original 8 m/s at 0.2 s to 12 m/s at 0.5 s in the form of a slope and drops to 8 m/s after keeping for a while, and the corresponding results are shown as in Fig. 8.

i_d and i_q behave similarly under gradient wind with step wind. Therefore, it is no longer necessary to provide an extensive description.

Based on the above analysis, the reliability of SMC-MPC under conventional wind conditions is verified. Next, the speed and dq current are simulated under a random wind condition to demonstrate the method's robustness in time-varying uncertain wind speed.

The above simulation results are carried out under random wind speed, and the dq current diagram can be obtained (see Figures 9 and 10): Under random wind speed conditions, the rotor speed quickly tracks the reference speed with almost no overshoot under the SMC-MPC control strategy, which has a great dynamic effect. The d-axis current fluctuation is not significant and has lower pulsation. It shows that the strategy has better robustness and stronger anti-turbulence. Secondly, the q-axis current can also track the reference current well, which verifies the great dynamic performance of this strategy again.

The above simulation is carried out without considering the parameter perturbation. However, parameter perturbations exist in the wind power system's operation process. According to the analysis of reference [31], the mismatch of the flux linkage will cause the actual q-axis current to fail to track the given value and worsen the q-axis tracking effect. The system's robustness decreases but has little impact on the d-axis current. The inductance mismatch mainly affects the tracking performance of the d-axis current and reduces the system's dynamic performance. The stator resistance mismatch has a minor effect on the system and only slightly reduces the dynamic tracking performance. The simultaneous mismatch of these three motor parameters will seriously impact dynamic tracking and robustness.

To verify the improved MRAS strategy used in this paper, the mismatch of the three parameters is simulated during the operation of the step wind speed. Since the integral sliding mode controller used in the speed loop is not sensitive to parameter perturbations, the speed loop is no longer considered. Only the q-axis current and its tracking in the current loop are analyzed.

At 0.6 s, the three parameters are perturbed: The flux linkage jumps from 0.175 Wb to 0.2 Wb; the inductance jumps from 0.002 H to 0.0022 H; the resistance jumps from 0.2 Ω to 0.15 Ω. Thus the q-axis current diagram is as in Fig. 11.

Before the parameter perturbation occurs, the q-axis current has a nice effect on tracking the reference current. Parameter perturbation occurs at 0.6 s, and the actual current deviates from the reference current and fluctuates wildly. As the changed parameters are identified again and reentered into the control system, the q-axis current is stabilized within 0.07 s. At the same time, the actual d-axis current has no apparent fluctuation and has been stable at about 0 A.

In the simulation model, the parameter mismatch causes the reference current to deviate from the original reference value while also causing the actual q-axis current to fluctuate. Secondly, parameter identification is also re-tracking the actual current to the reference value. The correction time is longer, and the calculation is slower. Since the adaptive law designed by the proportional integral method is used in MRAS, the identification curve has overshooted, a common problem with MRAS-based parameter identification. Supposing that the proportional-integral (PI) parameter is not set well. In that case, there will be an overshoot and a static error between the parameter identification estimate and the reference value, which will also slow down the identification speed and affect the identification accuracy. There is still room for improvement on this issue.

5. CONCLUSION

This paper aims at the problem that external wind speed disturbances and parameter perturbation affect the wind power system, which degrades the system's performance. The integral sliding mode controller is used to replace the speed loop, and the DPCC is used to replace the current loop. Meanwhile, a nonlinear extended state observer is designed for the speed loop to compensate for internal and external disturbances. An improving MRAS parameter identification model is designed for the current loop. The SMC-MPC strategy is proposed by analyzing the PMSM model in the dq coordinate system and then comparing it with the double-PI and double-MPC control. The simulation results show that the speed loop tracking and anti-disturbance ability under SMC-MPC control are significantly improved; the response speed is faster; the robustness is stronger. Under the current loop, the dynamic performance is better, and the control accuracy is higher, which realizes the wind power system's control performance and improves the effect of MPPT.

Finally, considering the adaptive law designed for the proportional-integral link used in MRAS, there is still room for further improvement to enhance the parameter identification.

REFERENCES

[1] Shi, K., Y. Chen, Z. He, J. Wang, and Y. Li, "Design of permanent magnet synchronous motor control system for electric vehicle air conditioning compressor based on vector control," *Open Access Library Journal*, Vol. 06, No. 1, 1–9, 2019.

[2] Yu, S., S. Zhong, H. Zhao, P. Xia, and K. Guo, "Calculation of circumferential modal frequencies of permanent magnet synchronous motor," *Journal of Harbin Institute of Technology (new Series)*, Vol. 26, No. 01, 81–91, 2019.

[3] Charalampidis, A., A. Chaniotis, and A. Kladas, "Current waveform optimization techniques for synchronous machines and numerical evaluation in the case of a pmsm wind turbine generator," *Electrical Engineering*, Vol. 99, No. 2, 1–9, 2018.

[4] Tarczewski, T., L. Grzesiak, A. Wawrzak, K. Karwowski, and K. Erwinski, "A state-space approach for control of npc type 3-level sine wave inverter used in foc pmsm drive," *Bulletin of The Polish Academy of Sciences Technical Sciences*, Vol. 62, No. 3, 2014.

[5] Zhao, H., C. Jiang-Zhou, and W. Jun-Li, "Research on mppt control for srg wind power generation system," *Chinese Journal of Power Sources*, 2016.

[6] Kalyan, R., J. Sharan, and M. Kumar, "Fuzzy logic control based pmsm drive by using svpwm," *Bulletin of The Polish Academy of Sciences Technical Sciences*, 2018.

[7] Dhivya, S. and S. Anitha, "Sensorless control of pmsm using sliding mode technique," *International Journal of Pure and Applied Mathematics*, Vol. 119, No. 12, 2159–2166, 2018.

[8] Gao, Y., Y. Wu, X. Wang, and Q. Chen, "Characteristic model-based adaptive control with genetic algorithm estimators for four-pmsm synchronization system," *International Journal of Control Automation and Systems*, No. 2, 2020.

[9] Xie, W., X. Wang, F. Wang, W. Xu, R. Kennel, D. Gerling, and R. Lorenz, "Finite-control-set model predictive torque control with a deadbeat solution for pmsm drives," *IEEE Transactions on Industrial Electronics*, Vol. 62, No. 9, 1–1, 2015.

[10] Li, P., S. Qiu, X. Zeng, L. Zhou, and H. Ze, "Sliding mode variable structure control technology used in doubly-fed induction generation system," *Proceedings of The CSU-EPSA*, 2017.

[11] Singh, M. and E. Kumar, "Optimization & control of pmsm based wind energy using pi and fuzzy logic controller," *Engering*, 2015.

[12] Oliveira, C. R., M. Aguiar, J. B. A. Monteiro, W. A. Pereira, G. Paula, and T. P. Almeida, "Vector control of induction motor using an integral sliding mode controller with anti-windup," *Journal of Control Automation and Electrical Systems*, Vol. 27, 169–178, 2016.

[13] Liu, C., G. Luo, W. Tu, and H. Wan, "Servo systems with double closed-loops based on active disturbance rejection controllers," *Proceedings of The Chinese Society of Electrical Engineering*, Vol. 37, No. 23, 7032–7039, 2017.

[14] Peng, L., M. Jian-Jun, L. Wen-Qiang, and Z. Zhi-Qiang, "Improved integral sliding mode control for a class of nonlinear uncertain systems," *Control and Decision*, 2009.

[15] Yang, M., L. Niu, H. Wang, and D. Xu, "Research on dynamic response of the current loop for pmsm with small inertia," *Electric Machines and Control*, 2009.

[16] Guzman-Guemez, J., D. Laila, and S. Sharkh, "State-space approach for modelling and control of a single-phase three-level npc inverter with svpwm," in *2016 IEEE Power and Energy Society General Meeting (pesgm)*, 1–5.

[17] Zanon, M. and T. Faulwasser, "Economic mpc without terminal constraints: gradient-correcting end penalties enforce asymptotic stability," *Journal of Process Control*, Vol. 63, 1–14, 2018.

[18] Xie, W., X. Wang, F. Wang, W. Xu, R. Kennel, D. Gerling, and R. Lorenz, "Finite-control-set model predictive torque control with a deadbeat solution for pmsm drives," *IEEE Transactions on Industrial Electronics*, Vol. 62, No. 9, 5402–5410, 2015.

[19] Yang, N., S. Zhang, X. Li, and X. Li, "A new model-free deadbeat predictive current control for pmsm using parameter-free luenberger disturbance observer," *IEEE Journal of Emerging and Selected Topics in Power Electronics*, Vol. 11, No. 1, 407–417, 2022.

[20] Vafaie, M., B. Dehkordi, P. Moallem, and A. Kiyoumarsi, "Improving the steady-state and transient-state performances of pmsm through an advanced deadbeat direct torque and flux control system," *IEEE Transactions on Power Electronics*, Vol. 32, No. 4, 2964–2975, 2016.

[21] Wang, Y., X. Wang, W. Xie, F. Wang, M. Dou, R. Kennel, R. Lorenz, and D. Gerling, "Deadbeat model-predictive torque control with discrete space-vector modulation for pmsm drives," *IEEE Transactions on Industrial Electronics*, Vol. 64, No. 5, 3537–3547, 2017.

[22] Lan, Z., B. Wang, C. Xu, and L. Li, "A novel three-vector model predictive current control for permanent magnet synchronous motor," *Proceedings of The CSEE*, Vol. 38, No. S1, 243–249, 2018.

[23] Xu, Y., M. Hu, Z. Yan, Y. Zhang, and H. Ma, "A three-vector-based model predictive flux control for pmsm drives," *Journal of Electrical Engineering and Technology*, Vol. 16, No. 5, 2673–2684, 2021.

[24] Niu, L., M. Yang, G. Wang, and D. Xu, "Research on the robust current control algorithm of permanent magnet synchronous motor based on deadbeat control principle," *Proceedings of The Csee*, 2013.

[25] Li, Z., G. Feng, C. Lai, D. Banerjee, W. Li, and N. Kar, "Current injection-based multi-parameter estimation for dual three-phase ipmsm considering vsi nonlinearity," *IEEE Transactions on Transportation Electrification*, Vol. 5, No. 2, 405–415, 2019.

[26] Li, X. and R. Kennel, "General formulation of kalman-filter based online parameter identification methods for vsi-fed pmsm," *IEEE Transactions on Industrial Electronics*, Vol. PP, No. 99, 1–1, 2020.

[27] An, X., G. Liu, Q. Chen, W. Zhao, and X. Song, "Adjustable model predictive control for ipmsm drives based on online stator inductance identification," *IEEE Transactions on Industrial Electronics*, Vol. 69, No. 4, 3368–3381, 2021.

[28] Xuliang, Y., H. Chengqi, W. Jingfang *et al.*, "A two-vector-based model predictive current control with online parameter identification for pmsm drives," *Proceedings of The Csee*, Vol. 12, No. 30, 1–13, 2022.

[29] Zeng, Z., L. Wu, Z. Yang *et al.*, "Self-learning sliding-mode disturbance rejection control for non-affine systems," *Control Theory & Applications*, Vol. 33, No. 7, 980–987, 2016.

[30] Huang, X., H. Pan, and K. Yuan, "Speed and current control of pmsm based on double mpc," in *2020 7th International Forum on Electrical Engineering and Automation (IFEEA)*, 300–304.

[31] Liu, Y., S. Cheng, Y. Zhao, J. Liu, and Y. Li, "Optimal two-vector combination-based model predictive current control with compensation for pmsm drives," *Taylor & Francis*, Vol. 106, No. 6, 880–894, 2019.